

PCCP

Accepted Manuscript



This is an *Accepted Manuscript*, which has been through the Royal Society of Chemistry peer review process and has been accepted for publication.

Accepted Manuscripts are published online shortly after acceptance, before technical editing, formatting and proof reading. Using this free service, authors can make their results available to the community, in citable form, before we publish the edited article. We will replace this *Accepted Manuscript* with the edited and formatted *Advance Article* as soon as it is available.

You can find more information about *Accepted Manuscripts* in the [Information for Authors](#).

Please note that technical editing may introduce minor changes to the text and/or graphics, which may alter content. The journal's standard [Terms & Conditions](#) and the [Ethical guidelines](#) still apply. In no event shall the Royal Society of Chemistry be held responsible for any errors or omissions in this *Accepted Manuscript* or any consequences arising from the use of any information it contains.

Kinetically Stabilized Aliovalent Europium-Doped Magnesium Oxide as UV Sensitized Phosphor

Cite this: DOI: 10.1039/x0xx00000x

Chandresh Kumar Rastogi^a, Sulay Saha^b, Sri Sivakumar^{a,b,c,*}, Raj Ganesh S Pala^{b,*} and Jitendra Kumar^{a,*}

Received 00th January 2012,
Accepted 00th January 2012

DOI: 10.1039/x0xx00000x

www.rsc.org/

Doping of size mismatched aliovalent ions is challenging due to its associated elastic and electronic stress making the thermodynamics unfavorable. Despite such features, its utilization may be viable if such systems can be made metastable by suppressing the kinetics of phase segregation. In light of such possibilities, we utilize sol-gel synthesis for preparing size mismatched trivalent europium doped MgO ($\text{Mg}_{1-x}\text{Eu}_x\text{O}:(x/2)V''_{\text{Mg}}$) system, which can be potentially used in optical applications. It is found that such doped system can be metastabilized and the extent of metastability can be correlated to critical temperature (T_c) required for phase segregation which decreases with the dopant concentration. For $x=0.005$, 0.01, and 0.02, T_c is above 1200 °C, 500-800 °C and less than 500 °C, respectively. As the synthesis temperature is 500 °C, these trends in critical temperatures make it impossible to metastabilize europium in MgO with $x>0.01$. Doping is evident from X-ray diffraction data, excitation spectra, high resolution emission spectra, and luminescence lifetimes. Characteristic strong red emission of Eu^{3+} has been observed via energy transfer from MgO matrix to Eu^{3+} . Density functional theory based simulations suggest stabilization of Eu^{3+} in MgO at lower doping concentration through formation of cation vacancies which is also evident from optical studies. Furthermore, thin film deposited using e-beam evaporation technique from $\text{Mg}_{1-x}\text{Eu}_x\text{O}:(x/2)V''_{\text{Mg}}$ ($x=0.005$) system shows UV sensitized emission with CIE coordinates (0.26, 0.21).

Introduction

Aliovalent doping is a powerful approach for modulating opto-electronic and catalytic properties.¹⁻³ However, the synthesis of size mismatched aliovalent doped system is a challenging task due to valency and size mismatch between the dopant and the host ions which introduces energy penalty.⁴⁻⁹ In response to valency and size mismatch, the doped systems try to minimize their energy via mechanisms like creation of anion or cation vacancy, interstitial defect, Frenkel pair, antisite, other defects and surface segregation of dopants.^{10,11} Specifically, creation of a vacancy provides an avenue for the release of elastic stresses and it may provide compensation for the aliovalency of the dopant. The presence of variable valence state of host cation (e.g. transition metal ions that can take up different charge state depending on the aliovalency of the dopant) also facilitates the electronic interaction with the dopant and stabilizes the system.^{1,12} On the other hand, aliovalent doping of ions (having fixed or variable valence state) in a host (comprised of ions having fixed valency) is expected to be more arduous. In such

systems, a dominant mechanism for increasing stability can be due to formation of vacancies, even though vacancy creation involves breaking of bonds.

If none of the stabilization mechanism is able to transform the doped system to the energetically favorable lowest energy state, then the dopant tends to move towards surface leading to surface doping or phase segregation. However, formation of the phase segregated state may involve large energy barriers making this a kinetically slow process, leading to the metastability of the doped system. The distribution of dopant from the bulk to surface may vary with the thermodynamics of dopant incorporation and kinetics associated with the diffusion of the dopant. Such kinetically metastabilized aliovalent size mismatched doped systems can generally be prepared via synthesis schemes wherein kinetic barrier cannot be overcome. One such method is the sol-gel synthesis which also has other advantages in terms of yielding products with high purity, homogeneity and composition control. In the sol-gel process, we anticipate the mixing of dopant and the matrix containing the host oxide to occur in the gel phase. Further, it is expected

that the gel is transformed to a doped oxide following hydrolysis, condensation and calcination at relatively low temperatures (compared to temperatures required for solid state synthesis). In contrast to certain synthetic schemes like deposition-precipitation, in the sol-gel synthesis the dopant is expected to be distributed both in the bulk and at the surface of the host oxide. Depending on whether the system is in equilibrium or in a metastable configuration, the distribution of the dopant will depend on energetic or kinetic factors.

We explored the aliovalent size mismatched lanthanide-ion doping in inorganic matrix (MgO) prepared via sol-gel route and explored whether the distribution of the dopant in the doped oxide is determined by the thermodynamics of the europium dopant incorporation into the MgO host oxide or by its kinetics. Lanthanide ions doping into inorganic matrices (e.g. oxides, vanadates, phosphates, fluorides) is particularly interesting since they possess superior optical properties (e.g. high lifetime).¹³ Among the inorganic matrices, MgO, can be a potential host for lanthanide-ion doping because of their applications in plasma display panels (phosphor as well as protective layer) and catalysis.^{1, 14} MgO possesses strong absorption band in the range 200–450 nm due to their defect states (e.g. F^0 and F^+ centers) which can be utilized to excite Ln^{3+} ions through energy transfer.^{15, 16} This indirect excitation of Ln^{3+} ions can be much more efficient than their direct excitation (absorption cross-section $\sim 10 \text{ cm}^{-1}$) because of their high absorption cross section.

In this regard, an extensive study focusing on X-ray diffraction data, lifetime estimation and excitation spectra, along with computationally obtained energetics will greatly enhance our understanding of the mechanism underlying the doping of Ln^{3+} in MgO host. Such a comprehensive study is unavailable in the existing literature and the present work attempts to fill this gap.¹⁷⁻²²

In the present study, Eu^{3+} -doped MgO have been characterized by X-ray diffraction, high resolution transmission electron microscopy (HRTEM), selected area electron diffraction (SAED) and optical characterization techniques. Spectroscopic characterizations by recording photoluminescence emission spectra, excitation spectra, luminescence decay curves and high resolution emission spectra at low temperature (78 K) as well as room temperature have been carried out for providing information about the valence state and the coordination of europium ions into MgO. The above mentioned experiments provide the evidence for doping of Eu^{3+} ions in MgO. The extent of surface and bulk doping is correlated with luminescence lifetime data by recording the decay curve. The contribution of the lifetime from the bulk state decreases as the doping concentration increases from $x=0.005$ to 0.01 which is indicative of increase in concentration of surface dopant.

To further explore the stability (or metastability) two kinds of studies were performed. First, synthesized doped oxides with different dopant concentration were heated to different temperatures to investigate the possibility of phase segregation of dopant. These studies suggest that the extent of metastability

varies inversely with the dopant concentration, wherein greater the temperature for phase segregation, more is the extent of metastability. Second, the energetics of dopant incorporation was explored in the absence and presence of Mg^{2+} vacancy by density functional theory (DFT) calculations. The energy calculation and Bader charge analysis suggest creation of cationic vacancy in the doped oxide ($\text{Mg}_{1-x}\text{Eu}_x\text{O}:(x/2)\text{V}''_{\text{Mg}}$) which is accompanied by the stabilization of trivalent Eu^{3+} state of the dopant. The energetics obtained via DFT simulations in combination with the experimental studies involving heat treatments to higher temperatures, suggests that the incorporation of Eu^{3+} ion into MgO is kinetically stabilized provided the synthesis is performed below the critical temperature beyond which the phase segregation occurs. Thin film prepared below this critical temperature using e-beam deposition technique shows near blue color emission upon excitation with UV light.

Experimental

Ethanol solutions of $\text{Mg}(\text{NO}_3)_2 \cdot 6\text{H}_2\text{O}$ (99.9 %, Qualigens fine chemicals, India) and oxalic acid (99.9 %, Rankem Chemicals, India) have been mixed together in the molar ratio of 1:1 and stirred well to form a gel which has been digested for 12 h and then dried at 100°C for 24 h to yield a white powder of magnesium oxalate dihydrate ($\text{MgC}_2\text{O}_4 \cdot 2\text{H}_2\text{O}$). The powder has been grounded and decomposed at 500°C for 2 h in air to produce MgO.²⁷ Ln^{3+} -doped MgO ($\text{Ln}^{3+}=\text{Eu}^{3+}; x=0.001-0.1$ and $\text{Tb}^{3+}; x=0.005$) have been synthesized with the above protocol using stoichiometric amount of $\text{Ln}(\text{NO}_3)_3 \cdot 5\text{H}_2\text{O}$ ($\text{Ln}^{3+}=\text{Eu}^{3+}$ and Tb^{3+} 99.9 %, Sigma-Aldrich) salt solution. In a similar manner Eu_2O_3 samples have been prepared. Ln^{3+} -doped MgO have been denoted as $\text{Mg}_{1-x}\text{Ln}_x\text{O}:(x/2)\text{V}''_{\text{Mg}}$ throughout the discussion, where V''_{Mg} refers to Mg^{2+} vacancies present in the system.

For preparation of thin films by e-beam evaporation, a pellet (diameter 10 mm, thickness ~ 5 mm) was produced from $\text{Mg}_{1-x}\text{Eu}_x\text{O}:(x/2)\text{V}''_{\text{Mg}}$ ($x=0.005$) nanopowder by cold pressing at a hydraulic pressure of ~ 80 kN using a die and sintered at 1000°C for 2 h to serve as a target. The pellet and a few cleaned quartz substrates of size 25 mm x 25 mm were then introduced in the work chamber and evacuation commenced. After attaining a pressure of $\sim 2 \times 10^{-6}$ mbar, thin films were deposited on quartz substrate by evaporation of material using a 6 kV electron beam at an emission current of 80 mA and annealed subsequently at 500°C for 2h in air.

The materials characterizations have been done using X-ray diffraction (XRD) technique, UV-Vis absorption, X-ray photoelectron (XPS), X-ray fluorescence (XRF), Fourier transform infrared (FTIR) and fluorescence spectroscopy, energy dispersive X-ray analysis (EDAX) and transmission electron microscopy (TEM). The details of experimental technique as well as computational methodologies have been given in ESI.

Results and Discussion

Formation of $\text{Mg}_{1-x}\text{Eu}_x\text{O}:(x/2)\text{V}''_{\text{Mg}}$

$\text{Mg}_{1-x}\text{Eu}_x\text{O}:(x/2)\text{V}''_{\text{Mg}}$ ($x=0-0.1$) samples were prepared by decomposition of dried oxalate gel at 500 °C for 2 h (as detected by TGA analysis, Fig. S1). Fig. 1a-d shows XRD patterns of $\text{Mg}_{1-x}\text{Eu}_x\text{O}:(x/2)\text{V}''_{\text{Mg}}$ ($x=0-0.02$). The pattern corresponding to compositions, $x=0-0.01$ matches well with the f.c.c. (NaCl-type) structure of MgO (JCPDS PDF No. 04-0829). However, Fig. 1d ($x=0.02$) shows additional peaks apart from MgO phase which is attributed to europium dioxycarbonate ($\text{Eu}_2\text{O}_2\text{CO}_3$) phase having tetragonal cell (JCPDS PDF No. 25-0334). However, it can be indexed better with an orthorhombic unit cell ($a\sim 5.87$ Å, $b\sim 5.65$ Å, $c\sim 12.98$ Å). This clearly suggests segregation of secondary phase for the compositions $x>0.01$. With addition of europium (up to $x=0.01$

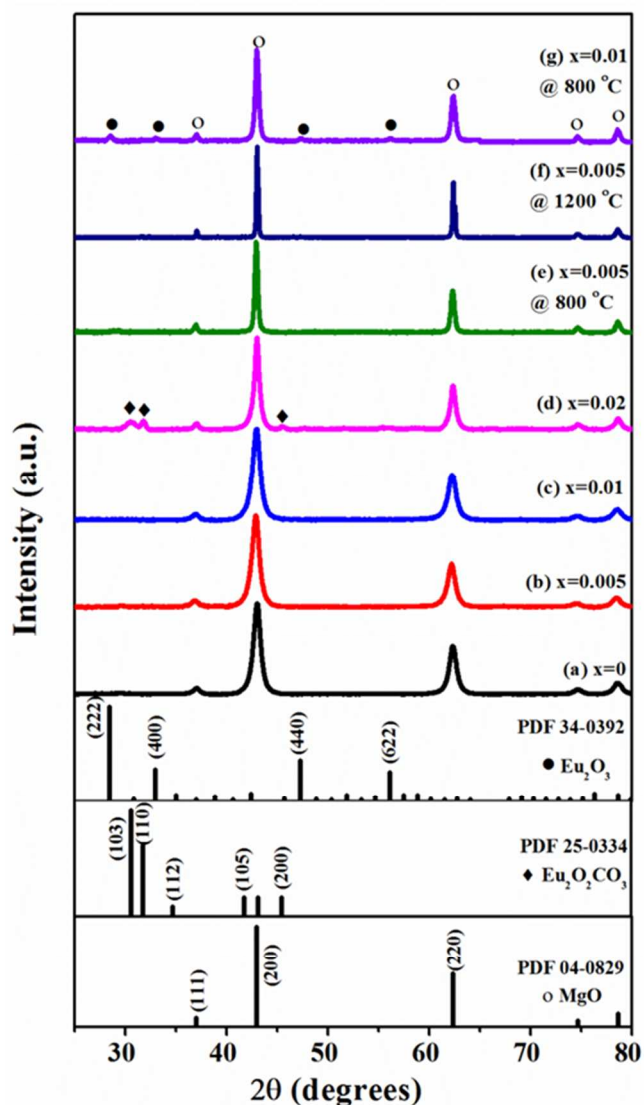


Fig. 1 XRD patterns of $\text{Mg}_{1-x}\text{Eu}_x\text{O}:(x/2)\text{V}''_{\text{Mg}}$ ($x=0-0.02$) samples (a-d) as prepared samples (e-g) heat treatment of as prepared samples at different temperature

at least), the samples continue to exhibit rocksalt MgO structure with marginal increase in the lattice parameter of MgO. The value being 4.212 Å for compositions $x=0.01$ against 4.206 Å

of undoped MgO suggesting presence of uniform strain due to doping. Since the size of Eu^{3+} ion is much larger than that of Mg^{2+} ion ($r_{\text{Eu}^{3+}}=0.96$ Å, $r_{\text{Mg}^{2+}}=0.72$ Å), the net increase in lattice parameter can be attributed to two competing effects: expansion caused by insertion of bigger Eu^{3+} ions at Mg^{2+} sites and contraction due to creation of vacancies. However, for the compositions $x>0.01$, the stress developed in the system due to size/charge mismatch can be high enough to develop the instability causing the phase segregation.

The average crystallite size (t) of samples has been deduced from Debye Scherrer formula $t=0.9\lambda/\beta\cos\theta$, where λ is the wavelength of X-rays and β is the full width at half maxima (FWHM) of diffraction peak at Bragg angle θ after correction for instrumental contribution (taking silicon as standard). The values of ' t ' are ~ 10 nm for $\text{Mg}_{1-x}\text{Eu}_x\text{O}:(x/2)\text{V}''_{\text{Mg}}$ ($x=0-0.01$) sample. The present studies clearly suggest that samples possessing composition $x\leq 0.01$ ($x>0.01$) does not (does) show phase segregation upon exposure to 500 °C. To explore possible metastability in the doped system for samples $x<0.01$, the samples were heat treated at higher temperature (>800 °C) and ambient pressure. XRD pattern of $\text{Mg}_{1-x}\text{Eu}_x\text{O}:(x/2)\text{V}''_{\text{Mg}}$ ($x=0.01$) sample heat treated at 800 °C for 2 h shows an additional phase corresponding to cubic Eu_2O_3 phase as shown in Fig. 1e (JCPDS PDF No. 34-0392). On the other hand XRD pattern corresponding to heat treated $\text{Mg}_{1-x}\text{Eu}_x\text{O}:(x/2)\text{V}''_{\text{Mg}}$ ($x=0.005$) sample at 1200 °C for 18 h shows no phase segregation (Fig. 1f). The sensitivity of the XRD instrument at lower doping concentration has been checked by recording the X-ray diffraction patterns of equivalent physical mixture of MgO and Eu_2O_3 powders corresponding to composition $x=0.005$. The pattern for physical mixture sample shows presence of both MgO and Eu_2O_3 phases (Fig. S2 of ESI) which proves that the instrument is sensitive enough to detect the phase segregation at $x=0.005$. The heat treatment of doped sample at higher temperature expels out the dopant from the host lattice suggesting that the doped system is kinetically stabilized at lower temperature. Further, the extent of kinetic stabilization can be correlated to a critical temperature above which phase segregation occurs. This critical temperature and hence, the extent of metastability gets reduced with increase in dopant concentration. These trends suggest a heuristic (illustrated in TOC graphic) for the preparation and utilization of metastabilized doped systems. For a given concentration of the dopant, it is possible to metastabilize a doped system if the synthesis and utilization occur below the critical temperature. For the system under consideration, $\text{Mg}_{1-x}\text{Eu}_x\text{O}:(x/2)\text{V}''_{\text{Mg}}$, for all x , the synthesis temperature is 500 °C. For $x=0.005$, the critical temperature is at least >1200 °C and if this material is utilized in any application operating within 1200 °C, the metastability will be retained. For $x=0.01$, while the critical temperature is between 500 °C to 800 °C, if the utilization is below 500 °C, the material will remain metastable/single phase and functional. Such utilization temperatures are often occur in heterogeneous catalysis, wherein doped oxides are used extensively.¹ In contrast, for $x=0.02$, the critical temperature is ≤ 500 °C and with the synthesis temperature being 500 °C,

metastable structure corresponding to $x=0.02$ is impossible to achieve.

Bright field transmission electron micrograph of $\text{Mg}_{1-x}\text{Eu}_x\text{O}:(x/2)\text{V}''_{\text{Mg}}$ ($x=0.005$) sample shown in Fig. 2a suggests that the nanoparticles are in the size range of ~ 20 nm (Fig. S3 exhibits digital photograph showing dispersion). Fig. 2b illustrates the corresponding selected area electron diffraction (SAED) pattern which contains rings corresponding to crystal planes of rocksalt MgO structure. The transmission electron micrograph and corresponding selected area electron diffraction (SAED) pattern of undoped MgO sample is shown in Fig. S4 of ESI. High resolution transmission electron micrograph

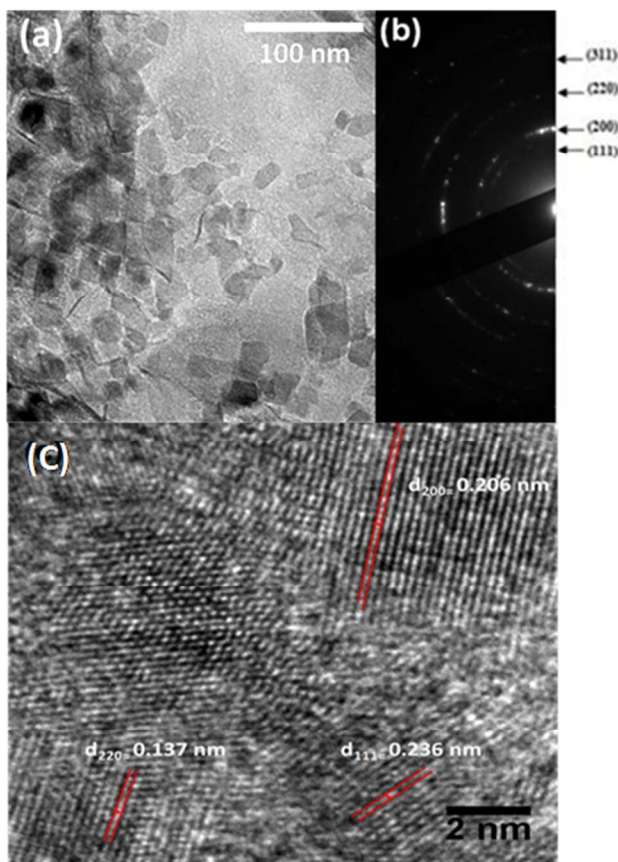


Fig. 2 (a) Transmission electron micrographs and (b) corresponding SAED pattern (c) HRTEM image of $\text{Mg}_{1-x}\text{Eu}_x\text{O}:(x/2)\text{V}''_{\text{Mg}}$ ($x=0.005$) sample

(HRTEM) of $\text{Mg}_{1-x}\text{Eu}_x\text{O}:(x/2)\text{V}''_{\text{Mg}}$ ($x=0.005$) sample (Fig. 2c) further proves the highly crystalline nature. The d-spacing corresponding to different planes (calculated from lattice fringes) match with the X-ray diffraction data. Further, XPS data (Fig. S5 of ESI) of $\text{Mg}_{1-x}\text{Eu}_x\text{O}:(x/2)\text{V}''_{\text{Mg}}$ ($x=0.01$) sample shows the Eu^{3+} concentration as ~ 0.6 atom % which nearly matches with the dopant:host cation concentration in the precursor. The binding energy (136.2 eV) of Eu 4d (inset in Fig. S5 of ESI) photo-electron is different from that of pure europium oxide (134.9 eV)²³ which rules out the possibility of phase segregation. In addition, the concentration of Eu^{3+} ion deduced from elemental mapping (Fig. S6) by energy dispersive X-ray analysis (EDAX) matches with that obtained

from X-ray fluorescence spectra (XRF) and XPS data. The atomic ratio of $\text{Eu}/(\text{Eu}+\text{Mg})$ deduced from EDAX mapping data (Table S1) is found to be ~ 0.011 . All the above facts suggest doping (up to $x=0.01$) of Eu^{3+} ions into MgO .

Optical and photoluminescence studies

Fig. 3 shows the UV-visible absorption spectra of $\text{Mg}_{1-x}\text{Eu}_x\text{O}:(x/2)\text{V}''_{\text{Mg}}$ ($x=0-0.05$) samples. The bands appearing in the wavelength range of 200–250 nm and 260–330 nm arise due to 4-fold (at corners) and 3-fold (at edges) coordinated O^{2-} ions, respectively.^{18, 24} Moreover, the broadening in the absorption band at 260–330 nm observed with increase in Eu^{3+} concentration may be attributed to changes in defect levels. The absorption peaks appearing at ~ 395 and 464 nm correspond to ${}^7\text{F}_0 \rightarrow {}^5\text{L}_6$ and ${}^7\text{F}_0 \rightarrow {}^5\text{D}_2$ transitions of Eu^{3+} ions. The FTIR spectra (Fig. S7 of ESI) of MgO and $\text{Mg}_{1-x}\text{Eu}_x\text{O}:(x/2)\text{V}''_{\text{Mg}}$ ($x=0.005$) samples depict a strong band at ~ 1457 cm^{-1} of

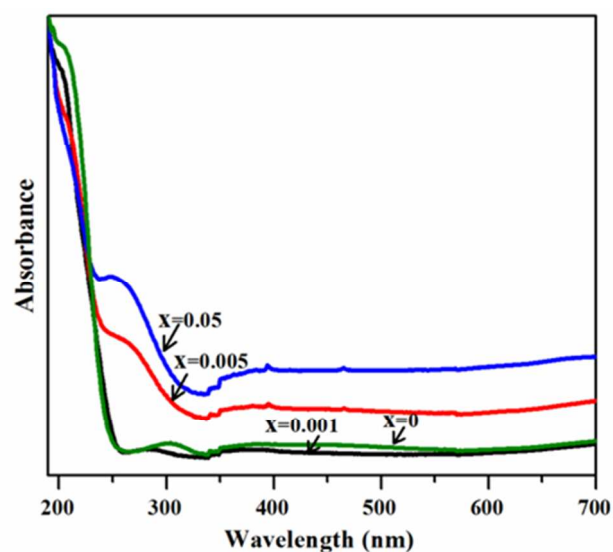


Fig. 3 UV-Vis absorption spectra of $\text{Mg}_{1-x}\text{Eu}_x\text{O}:(x/2)\text{V}''_{\text{Mg}}$ ($x=0-0.05$) sample

stretching vibration of $\text{Mg}-\text{O}$ while a shoulder at ~ 1640 cm^{-1} corresponds to $\text{O}-\text{H}$ bending mode of adsorbed water.²⁵ In addition, a sharp peak observed at ~ 3417 cm^{-1} is attributed to presence of hydroxyl group (OH) at low co-ordination sites or defects in MgO .²⁴ Fig. 4a-e shows the photoluminescence emission spectra of $\text{Mg}_{1-x}\text{Eu}_x\text{O}:(x/2)\text{V}''_{\text{Mg}}$ ($x=0.001-0.1$) samples recorded with excitation wavelength of 270 nm. The emission bands appearing around 577, 591, 615, 656 and 704 nm are associated with intra $4f^6$ transitions of Eu^{3+} ions.²⁶ The prominent emission peaks centered on ~ 615 nm and 704 nm (with a shoulder at 693 nm) are attributed to electric dipole transitions ${}^5\text{D}_0 \rightarrow {}^7\text{F}_2$ and ${}^5\text{D}_0 \rightarrow {}^7\text{F}_4$, respectively.²⁶ It is observed that the emission spectra of $\text{Mg}_{1-x}\text{Eu}_x\text{O}:(x/2)\text{V}''_{\text{Mg}}$ ($x \leq 0.01$) samples are similar (Fig. 4a-c) but different from others having compositions $x > 0.01$. In addition, the emission spectra depicted in Fig. 4d-e of compositions ($x > 0.01$) are similar to that of Eu_2O_3 samples (Fig. 4f) supporting thereby inference of the

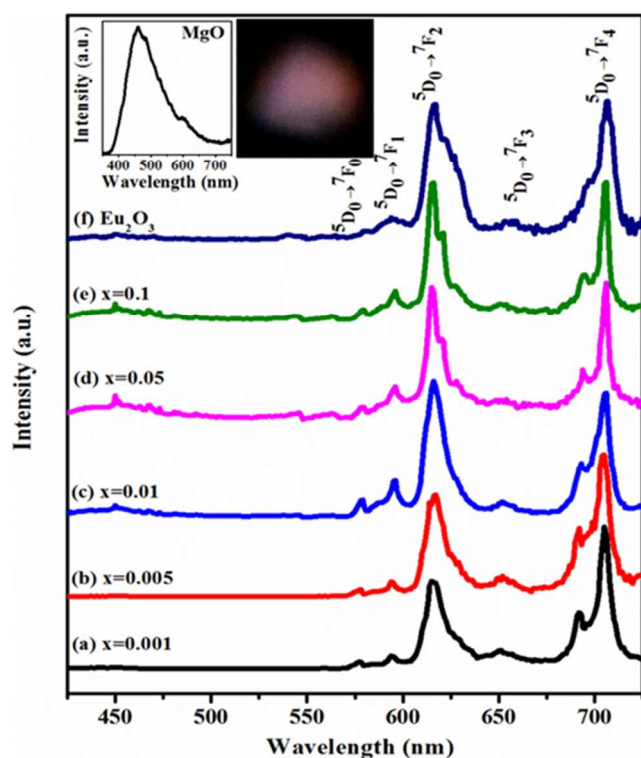


Fig. 4 Photoluminescence emission spectra of (a-e) $\text{Mg}_{1-x}\text{Eu}_x\text{O}:(x/2)\text{V}''_{\text{Mg}}$ ($x=0.001-0.1$), (f) Eu_2O_3 and MgO sample (in the inset) at the excitation wavelength 270 nm. A digital photograph of red color emission from $\text{Mg}_{1-x}\text{Eu}_x\text{O}:(x/2)\text{V}''_{\text{Mg}}$ ($x=0.005$) sample is also shown in inset

phase segregation. The weak emission peaks occurring at ~ 591 nm and ~ 656 nm are due to forbidden magnetic dipole transitions $^5\text{D}_0 \rightarrow ^7\text{F}_1$ and $^5\text{D}_0 \rightarrow ^7\text{F}_3$, respectively.²⁷ The strong electric dipole transitions combined with weak magnetic dipole transitions indicate lack of inversion symmetry prevailing around Eu^{3+} ions in the matrix with charge compensation locally by Mg^{2+} vacancy i.e. A-centers suggested in $\text{CaO}:\text{Eu}^{3+}$ system earlier.^{4, 28} The emission spectrum of undoped MgO samples (inset of Fig. 4) shows a broad emission band in the wavelength range 400-700 nm and attributed to point defects present.²⁹ The suppression of this emission band in doped samples may be due to energy transfer from MgO matrix to Eu^{3+} ions. Fig.4 (inset) also shows a typical digital photograph of red color emission from a sample having $x=0.005$ at the excitation wavelength of 270 nm. Similarly, $\text{Mg}_{1-x}\text{Tb}_x\text{O}:(x/2)\text{V}''_{\text{Mg}}$ ($x=0.005$) sample prepared in the same manner exhibits the characteristic emission of Tb^{3+} ions upon excitation with 270 nm UV radiation (Fig. S8 of ESI) with green color. Fig. 5 shows the excitation spectra of $\text{Mg}_{1-x}\text{Eu}_x\text{O}:(x/2)\text{V}''_{\text{Mg}}$ ($x=0.001-0.01$) samples for emission at 615 nm of $^5\text{D}_0 \rightarrow ^7\text{F}_2$ transition of Eu^{3+} ions. The intense broad band (250-330 nm) and a weak but sharp peak at ~ 395 nm are attributed to point defects of MgO and $^7\text{F}_0 \rightarrow ^5\text{L}_6$ transition of Eu^{3+} ions respectively.^{30, 31} Moreover, the intensity of 395 nm band increases with increase in doping concentration. The above results suggest efficient transfer of absorbed energy from MgO matrix to Eu^{3+} ions is indeed taking place to give rise

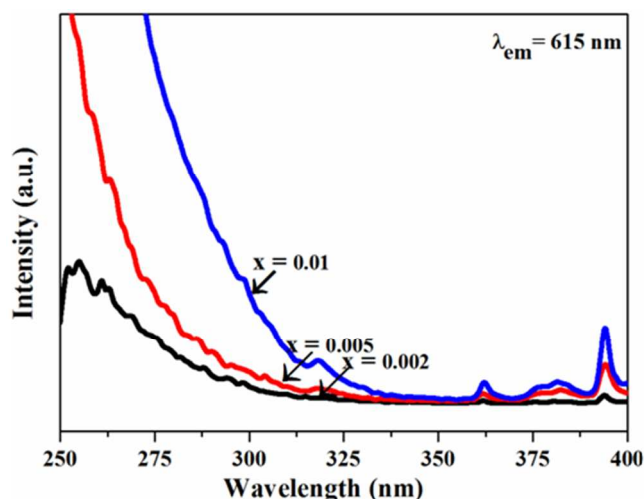


Fig. 5 Excitation spectra of $\text{Mg}_{1-x}\text{Eu}_x\text{O}:(x/2)\text{V}''_{\text{Mg}}$ ($x=0.001-0.01$) sample for emission at 615 nm

emission at 615 nm. This excitation band can only be realized if the energy transfer occurs from MgO matrix to Eu^{3+} ion and this can happen when the ions are in the bulk of the host. This fact also supports doping of Eu^{3+} ion into MgO . The effective luminescence lifetime of $^5\text{D}_0$ level of Eu^{3+} ions have been estimated by recording the decay curve of 615 nm emission and performing double exponential fitting described by equation 1¹⁸:

$$y = y_0 + A_1 \exp(-t_1/\tau_1) + A_2 \exp(-t_2/\tau_2) \quad (1)$$

where τ_1 and τ_2 are the time periods in which luminescence intensity falls to $1/e$ of its original value. The effective luminescence lifetime τ_{eff} is then given by:³²

$$\tau_{\text{eff}} = (A_1\tau_1^2 + A_2\tau_2^2)/(A_1\tau_1 + A_2\tau_2) \quad (2)$$

Fig.6a shows decay curves of $\text{Mg}_{1-x}\text{Eu}_x\text{O}:(x/2)\text{V}''_{\text{Mg}}$ ($x=0.005-0.1$) samples. The effective lifetime values estimated using equation 2 are found to be 1.8, 1.4 and 0.4 ms for compositions $x=0.005, 0.01, 0.1$ respectively. The decrease in the lifetime with increase in the doping concentration may be due to the following reasons: 1) concentration quenching, 2) increase in the concentration of Eu^{3+} ions in the surface, and 3) formation of separate phases. Table S2 shows the two components of the lifetime obtained after double exponential fitting of the recorded decay curve. The shorter component (τ_1) corresponds to the contribution from the surface doped Eu^{3+} ions while longer component (τ_2) has been attributed to the ions doped into bulk. The relative percentage of shorter component (A_1) increases from 51.74 to 67.22 % as the doping concentration increased from $x=0.005$ to 0.01 which suggests the presence of Eu^{3+} ions is more in surface compared to bulk. The estimated effective lifetime for composition $x=0.005$ is comparable to that of reported lifetime for Eu^{3+} ions doped in Y_2O_3 (2.0 ms),³³

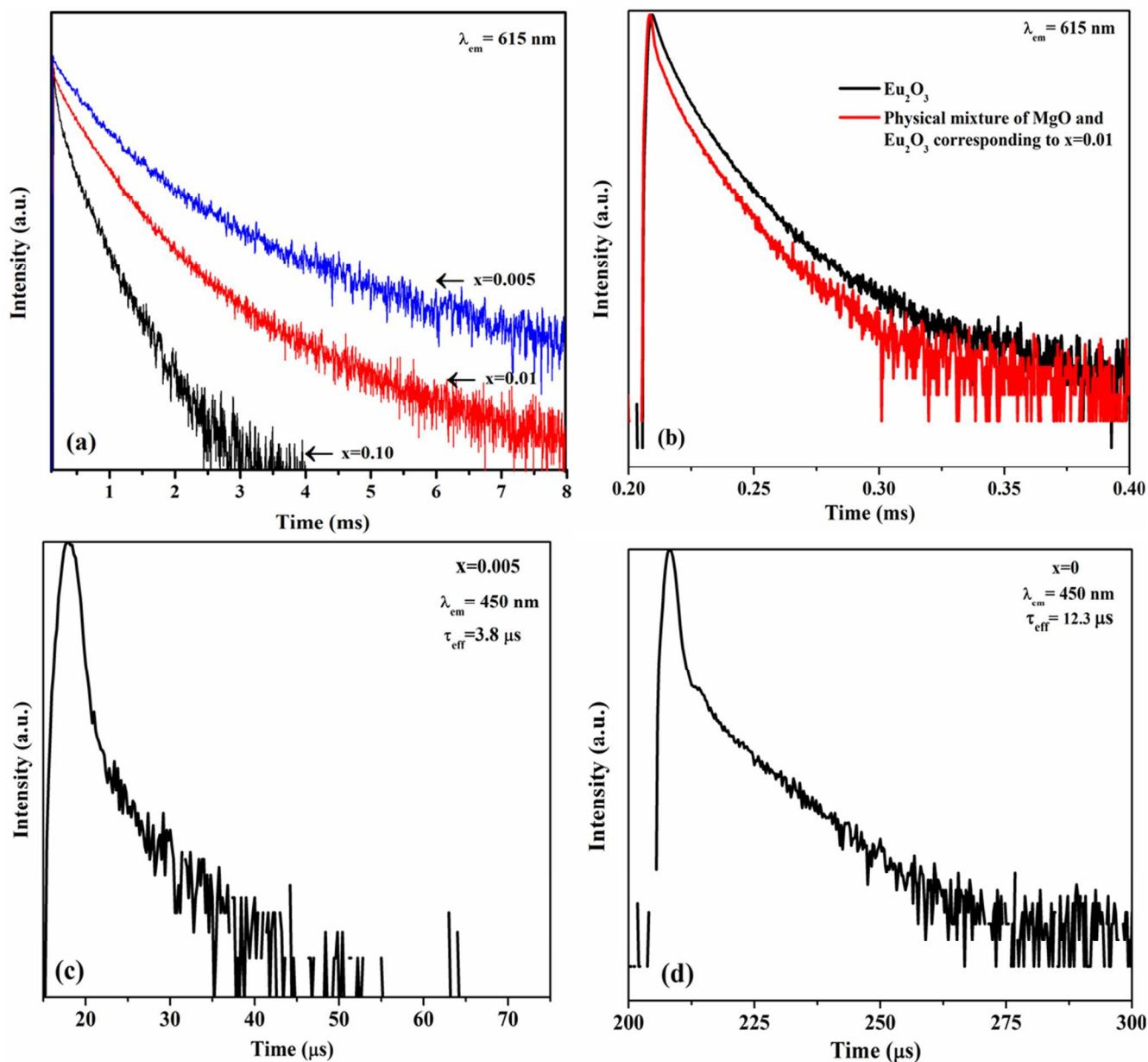


Fig. 6 Luminescence decay curve for 615 nm emission of Eu^{3+} ions in (a) $\text{Mg}_{1-x}\text{Eu}_x\text{O}:(x/2)\text{V}''_{\text{Mg}}$ ($x=0.005-0.10$) samples (b) Eu_2O_3 and physical mixture of MgO and Eu_2O_3 (c) Decay curve of 450 nm emission from host in $\text{Mg}_{1-x}\text{Eu}_x\text{O}:(x/2)\text{V}''_{\text{Mg}}$ ($x=0.005$) sample and (d) decay curve of 450 nm emission from undoped MgO

Gd_2O_3 (1.7 ms),³⁴ Lu_2O_3 (1.33 ms) matrices³⁵ etc. as mentioned in Table S3. Furthermore, quantum yield ($\eta\Gamma_{\text{rad}}$) has been estimated based on the observed lifetime value using equation 3 and is mentioned in Table S4.

$$\eta\Gamma_{\text{rad}} = \tau_{\text{obs}}/\tau_{\text{rad}} \quad (3)$$

where τ_{obs} and τ_{rad} are the observed and radiative lifetime of $^5\text{D}_0$ state of Eu^{3+} . We have taken the radiative lifetime (2.9 ms) from Eu^{3+} doped TiO_2 matrix which has similar phonon energy (766 cm^{-1}) to that of MgO (750 cm^{-1}).³⁶

The decay curves of pure Eu_2O_3 and physical mixture of pure MgO and Eu_2O_3 equivalent to $x=0.01$ (Fig. 6b) correspond

to lifetime values of 16.4 and 12.3 μs respectively, in contrast to milliseconds lifetime values obtained in the doped samples. The long luminescence lifetime observed in $\text{Mg}_{1-x}\text{Eu}_x\text{O}:(x/2)\text{V}''_{\text{Mg}}$ ($x<0.01$) samples is arising due to incorporation of Eu^{3+} ions into MgO matrix. Fig. 6c shows luminescence decay curves of 450 nm emissions from $\text{Mg}_{1-x}\text{Eu}_x\text{O}:(x/2)\text{V}''_{\text{Mg}}$ ($x=0.005$) samples while Fig. 6d corresponds to that of undoped MgO . The lifetime values estimated from decay curves are 3.8 μs and 12.3 μs for the doped and undoped cases respectively. The decrease in the lifetime of 450 nm emission in doped case supports the belief of energy transfer from MgO to Eu^{3+} ions. The energy transfer efficiency (η_T)

from MgO to Eu^{3+} ions has been calculated by the following equation and is found to be ~ 0.69 :

$$\eta_T = 1 - \tau/\tau_0 \quad (4)$$

where τ and τ_0 are luminescence lifetime of 450 nm emission of host MgO (sensitizer) in presence and absence of Eu^{3+} ions (activator).

In order to gather information about the environment around Eu^{3+} ions, high resolution emission spectra of $\text{Mg}_{1-x}\text{Eu}_x\text{O}:(x/2)\text{V}''_{\text{Mg}}$ ($x=0.005$) sample were recorded at 300 K and 80 K in the scan ranges 572-581 nm (${}^5\text{D}_0 \rightarrow {}^7\text{F}_0$ electric dipole transition of Eu^{3+}). The emission spectra shown in Fig.7

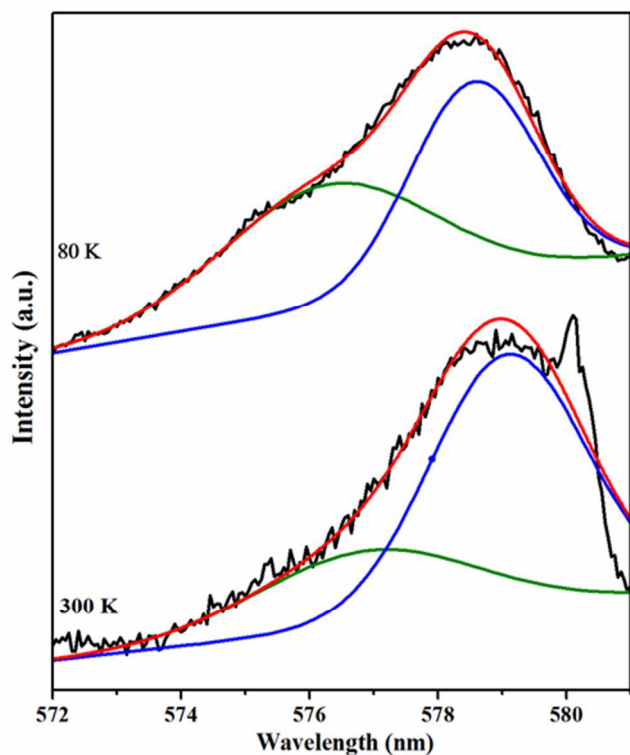


Fig. 7 High resolution emission spectra of $\text{Mg}_{1-x}\text{Eu}_x\text{O}:(x/2)\text{V}''_{\text{Mg}}$ ($x=0.005$) sample recorded at 300 K and 80 K obtained at excitation wavelength 270nm using 0.05 nm step size and 2s dwell time with 100 number of scans

comprise of two peaks centered at ~ 575.1 and 578.5 nm with the former becoming prominent and clearly visible at 80 K. This observation suggests that Eu^{3+} ions have two different environments in terms of coordination and/or distance of species in the matrix. Since the electric dipole transitions of Eu^{3+} ions are sensitive to environment, any local change would affect the corresponding emissions too. The emission peak at 575 nm becomes prominent by decrease of temperature due to suppression of thermally activated non-radiative transitions. Another emission peak appearing at 580.1 nm is attributed to artefacts.

DFT based Simulations Studies

The aliovalent europium doping in MgO matrix at low doping concentration ($x \sim 0.01$) with marginal lattice distortion is evident from above results. Phase segregation is observed for higher doping concentrations ($x > 0.01$) upon heating at high temperature ($> 500^\circ\text{C}$). Density functional theory (DFT) simulations have been performed to explore the trends in energetics and charge states of the dopant at different doping concentrations. Specifically, we consider both trivalent ($\text{Mg}_{1-x}\text{Eu}_x\text{O}:(x/2)\text{V}''_{\text{Mg}}$) and divalent ($\text{Mg}_{1-x}\text{Eu}_x\text{O}$) europium doping, with and without cation vacancies respectively, in MgO.

We have studied doping concentrations $x \sim 0.015$ -0.06 and doping concentration of $x \leq 0.001$ could not be explored due to limitations in computational resources available to us. The composition of $\text{Mg}_{1-x}\text{Eu}_x\text{O}$ ($x=0.015$) is represented within the periodic-DFT simulation using $4 \times 4 \times 2$ super-cell having 128 cation lattice sites (2 Eu and 126 Mg cations). In order to explore the stability of $\text{Mg}_{1-x}\text{Eu}_x\text{O}$ system, its relative energy has been compared with the products of decomposed and segregated oxide phases (MgO and Eu_2O_3). The decomposition of $\text{Mg}_{1-x}\text{Eu}_x\text{O}$ ($x=0.015$) in an oxygen rich atmosphere will result in the generation of 126 MgO units and a single Eu_2O_3 unit (Equation 2 and 4 of ESI). Such an analysis suggests that the decomposed and phase segregated state is more stable than the doped oxide by 7.6 eV.

In order to estimate the ionic size of europium in the rocksalt-type lattice, computations have been performed for rocksalt EuO and its lattice constant found to be 5.12 \AA . As this is larger than the lattice constant of MgO, it is expected that substitution doping of Eu in MgO will tend to expand the host lattice which will impose an elastic energy penalty. One method for relieving this elastic energy penalty is to create a cationic vacancy, with the expelled cation forming its oxide upon phase segregation. Even with the creation of cation (electron donor) vacancy, as the dopant has a greater valency than the host-oxide, electrons required for O anions (electron acceptor) might be compensated by the extra electron from the dopant. This kind of stabilization has been observed in studies on substitutional Cr doping in MgO.³⁷ This analogy has been utilized to quantify the possibility of existence of cation vacancies in europium doped MgO system.

In a system with cation (Mg^{2+}) vacancy, at a doping concentration corresponding to $x \sim 0.015$, the periodic super-cell containing 128 lattice sites, will contain 2 europium dopants, 125 Mg cations and 128 oxygen anions. The cationic vacancies have been created at the next to nearest neighbor (NNN) lattice site assuming the lattice distortion induced by europium substitution is predominantly confined to nearest neighbor (NN) oxygen atoms. Within the computational framework, the decomposition and phase segregation of $\text{Mg}_{1-x}\text{Eu}_x\text{O}:(x/2)\text{V}''_{\text{Mg}}$ with cation vacancy will generate 125 bulk MgO units and 1 unit of Eu_2O_3 (equation 1 and 3 in ESI). Such an analysis suggests that $\text{Mg}_{1-x}\text{Eu}_x\text{O}:(x/2)\text{V}''_{\text{Mg}}$ (with cation vacancy) is less stable than phase segregated phase, by 3.2 eV. It is found that even after the creation of cation vacancy, the doped structure ($\text{Mg}_{1-x}\text{Eu}_x\text{O}:(x/2)\text{V}''_{\text{Mg}}$) has residual expansive stress associated with it and this is exemplified by increase in lattice constant (by

0.015 Å) compared to pure MgO phase. This observation is validated by experimental results wherein marginal lattice expansion (by 0.01 Å) has been observed. The creation of cation vacancy in doped oxide ($\text{Mg}_{1-x}\text{Eu}_x\text{O}$) is favorable by -5.6 eV as opposed to 8.1 eV in undoped MgO in an oxygen rich environment. This suggests that the cationic vacancy formation is more favorable in the doped oxide than that of pure MgO. Further, the introduction of cation vacancy has decreased the relative instability of the doped oxide (from 7.6 to 3.2 eV) with respect to the decomposed and segregated phase of Eu_2O_3 and MgO. These computational results in conjunction with the results of the experimental studies suggest that the stability of the doped oxide is not due to its thermodynamics but due to high activation energy associated with kinetic pathway that prevents its decomposition and segregation.

Higher doping concentration leads to increased destabilization of the doped system as the relative energetic state of the decomposed and segregated constituent oxide decreases (Table S5). This suggests that it will be difficult to achieve kinetic stabilization at higher doping concentration as is also evident from experimental studies. Charge partition analyses have been utilized to correlate the experimentally observed charge state of europium ions to the Bader charge obtained within the DFT simulations. The computed formal charge is the difference between charge due to valence electrons and Bader charge, and this is compared with the experimentally observed charge state. In europium doped MgO system without cation vacancy, the formal charge on doped europium ion in MgO is +1.3. In contrast, with cation vacancy

case, the formal charge is +1.7. The formal charge on divalent europium in EuO is +1.4 in contrast to +1.8 for trivalent europium in Eu_2O_3 . It is observed that the formal charge on europium (+1.3) in doped MgO without cation vacancy is closer to that of divalent europium (+1.4) in EuO. However, the formal charge on europium (+1.7) in doped MgO with cation vacancy is closer to that of trivalent europium (+1.8) in Eu_2O_3 . These results agree well with trivalent europium incorporation as observed in photoluminescence studies.

Thin film for solid state lighting application

In order to show the applicability of the Eu^{3+} -doped MgO system, we have fabricated thin films derived from $\text{Mg}_{1-x}\text{Eu}_x\text{O}:(x/2)\text{V}''_{\text{Mg}}$ ($x=0.005$) sample which can be potentially used in solid state lighting application. Fig. 8a illustrates the emission spectrum of a typical $\text{Mg}_{1-x}\text{Eu}_x\text{O}:(x/2)\text{V}''_{\text{M}}$ ($x=0.005$) thin film deposited by e-beam evaporation method. It contains peaks at ~577, 591, 615, 649 and 704 nm arising due to $^5\text{D}_0 \rightarrow ^7\text{F}_J$ (where $J=0, 1, 2, 3$ and 4) transitions of Eu^{3+} ions and a broad band centered at ~430 nm attributed to defect states of host MgO. The luminescence arises from thin film possess the CIE coordinates of (0.26, 0.21) as shown in Fig. 8b. The luminescence lifetime of $^5\text{D}_0$ level of Eu^{3+} ions was estimated by double exponential fitting of decay curve shown in Fig. 8c and is found to be 0.58 ms. The luminescence characteristics of thin film is different from Eu^{3+} -doped nanopowders which may be due to the various defects present in the thin film during deposition.

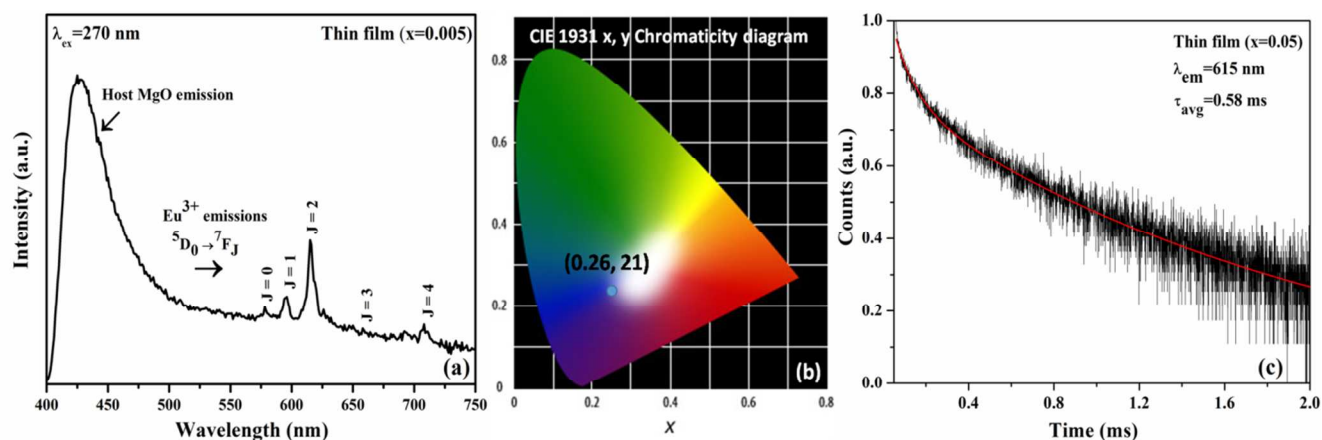


Fig. 8 (a) Emission spectrum at excitation wavelength 270 nm (b) CIE chromaticity diagram and (c) decay curve monitoring 615 nm emission of e-beam deposited $\text{Mg}_{1-x}\text{Eu}_x\text{O}:(x/2)\text{V}''_{\text{Mg}}$ ($x=0.005$) thin film

Conclusions

The broader objective of the present work is to explore the possibility of stabilizing (or metastabilizing) charge and size mismatched dopants in a host, which is especially difficult if the host does not have ions that can adopt variable valency. We

have specifically investigated europium doping in MgO host as it may find application in optical devices. Sol-gel synthesis at 500 °C has been adopted for all the doping concentration. It is found that $\text{Mg}_{1-x}\text{Eu}_x\text{O}:(x/2)\text{V}''_{\text{Mg}}$ samples for $x=0.005$ is metastable without phase segregation till $T=1200$ °C. However, for $x=0.01$ and $x=0.02$, phase segregation occurs at $T=800$ °C and $T<500$ °C respectively. This suggests that metastability of

the doped system is correlated to critical temperature (T_c) required for phase segregation which decreases with the dopant concentration. If the critical temperature is above synthesis temperature, metastable doped systems are feasible. The doping is visualized from the excitation spectra which suggest energy transfer from MgO matrix to doped Eu^{3+} ions. Furthermore, high resolution spectra recorded at low temperature, and luminescence lifetime data confirm the doping. In addition, the density functional theory based calculations suggest that the metastability of the system is achieved by the formation of cationic Mg^{2+} vacancies with marginal lattice expansion. Bader charge analysis also supports the presence of trivalent state of europium in MgO which is evident from the luminescence

studies. Additionally, thin films fabricated using e-beam evaporation method displays luminescence having CIE coordinates (0.26, 0.21) demonstrates its usefulness as phosphor in optical device.

Acknowledgements

SS is grateful to Department of Science and Technology (DST/CHE/20090220), Govt. of India for providing the funding for research. Thanks are due to DST for funding the Thematic Unit of Excellence. Authors are thankful to High Performance Computational Facility (HPC) at IIT Kanpur for providing the computational time

Notes and references

^aMaterials Science Programme, IIT Kanpur, Kanpur, India. ^bDepartment of Chemical Engineering, IIT Kanpur, Kanpur, India

^cCentre for Environmental Science and Engineering, IIT Kanpur, Kanpur, India

Fax: 91-512-2590104; Tel: 91-512-2897697; E-mail: srisiva@iitk.ac.in, rpala@iitk.ac.in, jk@iitk.ac.in

† Electronic Supplementary Information (ESI) available: Materials characterization techniques, computational methodology, heat of formation table, TGA, XRD of control samples, XPS and FTIR data. See DOI: 10.1039/b000000x/

- 1 E. W. McFarland and H. Metiu, *Chem. Rev.*, 2013, 113, 4391-4427.
- 2 S. Singh and M. S. R. Rao, *Phys. Rev. B*, 2009, 80, 045210-045210.
- 3 T. Takata and K. Domen, *J. Phys. Chem. C*, 2009, 113, 19386-19388.
- 4 D. Van der Voort, A. Imhof and G. Blasse, *J. Solid State Chem.*, 1992, 96, 311-317.
- 5 L. Armelao, G. Bottaro, M. Pascolini, M. Sessolo, E. Tondello, M. Bettinelli and A. Speghini, *J. Phys. Chem. C*, 2008, 112, 4049-4054.
- 6 A. Yanes, *Appl. Phys. Lett.*, 2004, 85, 2343-2345.
- 7 Y. Liu, W. Luo, R. Li, G. Liu, M. R. Antonio and X. Chen, *J. Phys. Chem. C*, 2008, 112, 686-694.
- 8 C. Hazra, S. Sarkar, B. Meesaragandla and V. Mahalingam, *Dalton Trans.*, 2013, 42, 11981-11986.
- 9 A. Kar and A. Patra, *J. Phys. Chem. C*, 2009, 113, 4375-4380.
- 10 D. Q. Fang, A. L. Rosa, R. Q. Zhang and T. Frauenheim, *J. Phys. Chem. C*, 2010, 114, 5760-5766.
- 11 W. Lee, J. W. Han, Y. Chen, Z. Cai and B. Yildiz, *J. Am. Chem. Soc.*, 2013, 135, 7909-7925.
- 12 M. Nolan, *J. Phys. Chem. C*, 2011, 115, 6671-6681.
- 13 J. C. G. Bünzli, *Chem. Rev.*, 2010, 110, 2729-2755.
- 14 J. Boeuf, *J. Phys. D: Appl. Phys.*, 2003, 36, R53.
- 15 P. Rinke, A. Schleife, E. Kioupakis, A. Janotti, C. Rödl, F. Bechstedt, M. Scheffler and C. G. Van de Walle, *Phys. Rev. Lett.*, 2012, 108, 126404.
- 16 Z. Yan, S. Chinta, A. A. Mohamed, J. P. Fackler and D. W. Goodman, *J. Am. Chem. Soc.*, 2005, 127, 1604-1605.
- 17 J. Alarcon, D. van der Voort and G. Blasse, *Mater. Res. Bull.*, 1992, 27, 467-472.
- 18 L. Peng, Y. Wang, Z. Wang and Q. Dong, *Appl. Phys. A: Mater. Sci. Process.*, 2011, 102, 387.
- 19 P. B. Devaraja, D. N. Avadhani, S. C. Prashantha, H. Nagabhushana, S. C. Sharma, B. M. Nagabhushana, H. P. Nagaswarupa and H. B. Premkumar, *Spectrochim. Acta A*, 2014, 121, 46-52.
- 20 F. Gu, S. F. Wang, M. K. Lü, W. G. Zou, G. J. Zhou, D. Xu and D. R. Yuan, *J. Cryst. Growth*, 2004, 260, 507-510.
- 21 F. Gu, C. Zhong Li and H. Bo Jiang, *J. Cryst. Growth*, 2006, 289, 400-404.
- 22 F. Gu, C. Li, H. Cao, W. Shao, Y. Hu, J. Chen and A. Chen, *J. Alloy Comp.*, 2008, 453, 361.
- 23 F. Mercier, C. Alliot, L. Bion, N. Thromat and P. Toulhoat, *J. Electron. Spectrosc. Relat. Phenom.*, 2006, 150, 21.
- 24 M. Sterrer, T. Berger, O. Diwald and E. Knözinger, *J. Am. Chem. Soc.*, 2002, 125, 195-199.
- 25 J. Singh, M. S. L. Hudson, S. K. Pandey, R. S. Tiwari and O. N. Srivastava, *Int. J. Hydrogen Energy*, 2012, 37, 3748-3754.
- 26 J. Huang, J. Xu, H. Li, H. Luo, X. Yu and Y. Li, *J. Solid State Chem.*, 2011, 184, 843-847.
- 27 H. Song, J. Wang, B. Chen, H. Peng and S. Lu, *Chem. Phys. Lett.*, 2003, 376, 1-5.
- 28 L. C. Porter and J. C. Wright, *J. Chem. Phys.*, 1982, 77, 2322-2329.
- 29 A. Kumar, S. Thota, S. Varma and J. Kumar, *J. Lumin.*, 2011, 131, 640-648.
- 30 Y. Uenaka and T. Uchino, *Phys. Rev. B*, 2011, 83, 195108-195115.
- 31 H. Wang, M. Uehara, H. Nakamura, M. Miyazaki and H. Maeda, *Adv. Mater.*, 2005, 17, 2506-2509.

- 32 N. Yaiphaba, R. S. Ningthoujam, N. S. Singh, R. K. Vatsa, N. R. Singh, S. Dhara, N. L. Misra and R. Tewari, *J. Appl. Phys.*, 2010, 107, 034301-034309.
- 33 T. Myint, R. Gunawidjaja and H. Eilers, *J. Phys. Chem. C*, 2011, 116, 1687-1693.
- 34 M. L. Debasu, D. Ananias, A. G. Macedo, J. Rocha and L. s. D. Carlos, *J. Phys. Chem. C*, 2011, 115, 15297-15303.
- 35 J. Yang, C. Li, Z. Quan, C. Zhang, P. Yang, Y. Li, C. Yu and J. Lin, *J. Phys. Chem. C*, 2008, 112, 12777-12785.
- 36 M. Chen and D. Goodman, *Science*, 2004, 306, 252-255.
- 37 F. Stavale, X. Shao, N. Nilius, H. J. Freund, S. Prada, L. Giordano and G. Pacchioni, *J. Am. Chem. Soc.*, 2012, 134, 11380-11383.